Stephen A. Boppart, MSEE
Brett E. Bouma, PhD
Costas Pitris, MSEE
Gary J. Tearney, PhD
James F. Southern, MD, PhD
Mark E. Brezinski, MD, PhD
James G. Fujimoto, PhD

Index terms:
Blood vessels, stenosis or obstruction, 92.92, 9*.721[2], 9*.92[2]
Lasers
Nerves, injuries, 40.40, 40.92
Optical coherence tomography, 9*.1299[2]
Surgery

Radiology 1998; 208:81–86

Abbreviations:
OCT = optical coherence tomography
2D = two-dimensional
3D = three-dimensional

[1] From the Dept of Electrical Engineering and Computer Science, Research Laboratory of Electronics, Massachusetts Institute of Technology, 77 Massachusetts Ave, Rm 36-345, Cambridge, MA 02139 (S.A.B., B.E.B., C.P., G.J.T., J.G.F.); Div of Health Sciences and Technology, Harvard–Massachusetts Institute of Technology (S.A.B., C.P.); Dept of Pathology, Children's Hospital, Boston (J.F.S.); and Cardiac Unit, Massachusetts General Hospital and Harvard Medical School (M.E.B.). Received Oct 1, 1997; revision requested Dec 24; revision received Jan 20, 1998; accepted Mar 3. Supported in part by grants from Office of Naval Research Medical Free Electron Laser Program grant (N00014-94-1-0717), U.S. Air Force Office of Scientific Research grant (F49620-95-1-0221), and U.S. Air Force Palace Knight Program; National Institutes of Health contracts NIH-9-RO1-EY11289-11 (J.G.F), NIH-1-R01-CA75289-01 (J.G.F., M.E.B.), and NIH-1-R29-HL55686-01A1 and NIH-RO1-AR44812-01 (M.E.B.); and Whittaker Foundation contract 96-0205 (M.E.B.).
Address reprint requests to S.A.B.

[2] 9*, Vascular system, location unspecified

Author contributions:
Guarantors of integrity of entire study, S.A.B., J.G.F., M.E.B.; study concepts, S.A.B., M.E.B.; study design, S.A.B., J.G.F.; definition of intellectual content, S.A.B., M.E.B.; literature research, M.E.B.; experimental studies, S.A.B., B.E.B., G.J.T.; data acquisition, S.A.B., C.P., J.F.S.; data analysis, S.A.B.; manuscript preparation, S.A.B.; manuscript editing, S.A.B., M.E.B., J.G.F.; manuscript review, M.E.B., J.G.F.

Intraoperative Assessment of Microsurgery with Three-dimensional Optical Coherence Tomography[1]

PURPOSE: To evaluate three-dimensional optical coherence tomography (OCT) for use in the assessment of the microsurgical anastomoses of vessels and nerves.

MATERIALS AND METHODS: OCT is an optical analogue of ultrasonography and is capable of imaging nontransparent biologic tissue by detecting backscattered infrared light. Cross-sectional in vitro images of rabbit and human vessels and nerves were obtained in as little as 125 msec at 10-μm resolution by using a solid-state laser as a light source. A surgical microscope was integrated with OCT to perform simultaneous imaging with en face visualization. Cross-sectional images were assembled to produce three-dimensional reconstructions of microsurgical specimens.

RESULTS: Three-dimensional OCT reconstructions depicted the structure within an arterial anastomosis and helped identify sites of luminal obstruction. The longitudinal spatial orientation of individual nerve fascicles was tracked in three dimensions to identify changes in position. In vitro human arteries and nerves embedded in highly scattering tissue and not visible at microscopy were located and imaged with OCT at eight frames per second.

CONCLUSION: The three-dimensional, micrometer-scale, diagnostic imaging capabilities of OCT permit rapid feedback for assessment of microsurgical procedures. OCT technology can be readily integrated with surgical microscopes and has potential for intraoperative monitoring to improve patient outcome.

Optical instruments have become well integrated into the surgical setting to visualize tissue and improve patient outcome. Surgical microscopes and loupes magnify tissue to help prevent iatrogenic injury and guide delicate surgical techniques. The repair of injured vessels and nerves is necessary to restore sensory and motor function after traumatic injury (1). Although the repair of sensitive structures is performed with the aid of surgical microscopes and loupes to magnify the surgical field (2), surgeons are limited to the en face view that these devices provide. A technique capable of subsurface, three-dimensional (3D), micrometer-scale imaging in real-time would permit the intraoperative monitoring of microsurgical procedures, offering immediate feedback to the surgeon and likely improvement in patient outcome.

Optical coherence tomography (OCT) is an optical imaging technology (3) ideally suited for the rapid acquisition of micrometer-scale–resolution two-dimensional (2D) and 3D images of biologic tissues such as small vessels and nerves. OCT was first used to image the transparent structures of the human eye (4,5) and has been used to help diagnose and track various macular diseases in a clinical setting (5,6). More recently, the use of longer wavelengths, which are absorbed and scattered less in biologic tissue, has permitted imaging in nontransparent tissues (7–9), for example, in the preliminary assessment of vessels and nerves (10). OCT is well suited for integration with medical and surgical optical instruments, and imaging has been performed with a radial-imaging, flexible catheter-endoscope (11), as well as a handheld surgical probe and laparoscope (12). Recently, catheter-endoscope–based OCT imaging of the gastrointestinal and respiratory tracts has been demonstrated in vivo in an animal model (13). OCT can function as a type of "optical

biopsy" by permitting the in vivo imaging of biologic morphology with micrometer-scale resolution without the need to excise and process a tissue specimen as in conventional biopsy.

The purpose of this study was to determine the capabilities of OCT for the intraoperative assessment of microsurgical procedures. We integrated the high-speed OCT technology with a surgical microscope and performed micrometer-scale 3D imaging of microsurgical specimens.

MATERIALS AND METHODS

OCT is a noninvasive imaging technology that does not necessitate contact with tissue; it works on the principle of the detection of optical backscatter of near-infrared light from biologic tissue (3,6). The technique is somewhat analogous to ultrasound (US) B-mode imaging, except reflections of light are detected rather than those of sound. Whereas ultrasound pulse propagation and detection can be described in terms of time delays, the echo delay time of light returning to the OCT instrument from the specimen cannot be measured directly with electronic methods due to the high speeds associated with the propagation of light. Therefore, a technique known as interferometry is used, in which a reference and a sample arm are used. A schematic of the instrument is shown in Figure 1. A chromium (Cr^{4+}):forsterite laser is used as a low-coherence light source for OCT imaging (14). Because the infrared imaging beam (wavelength, 1,280 nm) cannot be seen, a visible aiming beam (wavelength, 632 nm) is combined for guidance and tissue registration. The imaging beam is split in equal parts by means of a fiberoptic coupler, with half the beam sent to the reference arm and half sent to the sample arm of the fiberoptic Michelson interferometer.

Two configurations are shown in Figure 1. The first configuration (Fig 1, *A*) was used for in vitro imaging of rabbit arteries and nerves. The reference arm contained a mirror on a mechanical translating galvanometer to perform axial scanning. The position of the reference arm mirror was used to set the depths at which backscatter would be measured, because interference between the two arms only occurs when their path lengths are matched to within the coherence length of the laser source. The imaging beam in the sample arm was focused by means of a lens to a 30-μm-diameter spot, which corresponds to a 1.1-mm depth of field. The spot size determined the transverse resolution of the image, and the axial resolution was determined by means of the coherence length of the laser source. The laser source has a center wavelength of approximately 1,280 nm and provides an axial resolution of 10 μm.

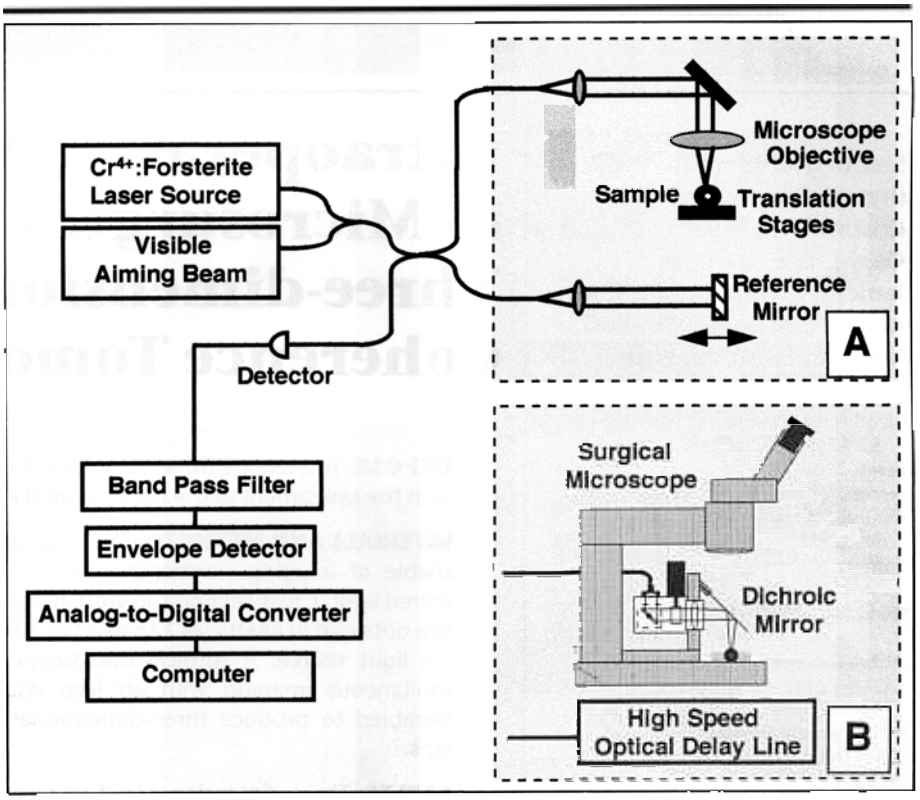

Figure 1. Schematic of the OCT instrument and surgical microscope shows two imaging configurations that use a Cr^{4+}:forsterite laser source. *A,* Configuration used to acquire cross-sectional and 3D images of microsurgical specimens: Sample arm includes a fixed microscope objective and micrometer-precision, computer-controlled stages to translate specimens. Reference arm mirror scanning is performed with a mechanical galvanometer. *B,* Configuration used for high-speed data acquisition: Specimens are imaged and visualized simultaneously with an integrated surgical microscope.

The specimens to be imaged were placed on a 2D micrometer-precision translational stage used to position and translate the specimen under a stationary imaging beam. Reflections from each arm were combined and detected with a photodiode. The reference arm mirror was translated at a known linear velocity. This translation imparts a Doppler shift to the reflected light. The electronic detection filter, with a center frequency at this known Doppler shift frequency, permits a high sensitivity and dynamic range (110 dB).

The second configuration (Fig 1, *B*) was used for in vitro imaging of human arteries and nerves at high speeds through a surgical microscope. The reference arm contained a high-speed optical delay line to permit more rapid axial imaging (13). The fiber of the sample arm was connected to a surgical microscope that had been modified for the simultaneous performance of OCT imaging and en face visualization. The infrared imaging beam and the visible aiming beam were directed by means of a pair of orthogonal galvanometer scanners to a focusing lens. A dichroic mirror coated to reflect the imaging and aiming beams was used to align the beams with the viewing axis of the microscope and to direct the beams onto the specimen. The OCT imaging beam was focused to a 30-μm-diameter spot, which corresponds to a 1.1-mm depth of field. The working distance of 60 mm beneath the dichroic mirror provided ample room for manual manipulation of microsurgical specimens. The specimen and image location were viewed through the microscope with the eye or were digitally imaged with a charge-coupled–device camera.

To demonstrate the use of OCT imaging for help in the diagnostic assessment of microsurgical procedures, in vitro microsurgical specimens were first acquired

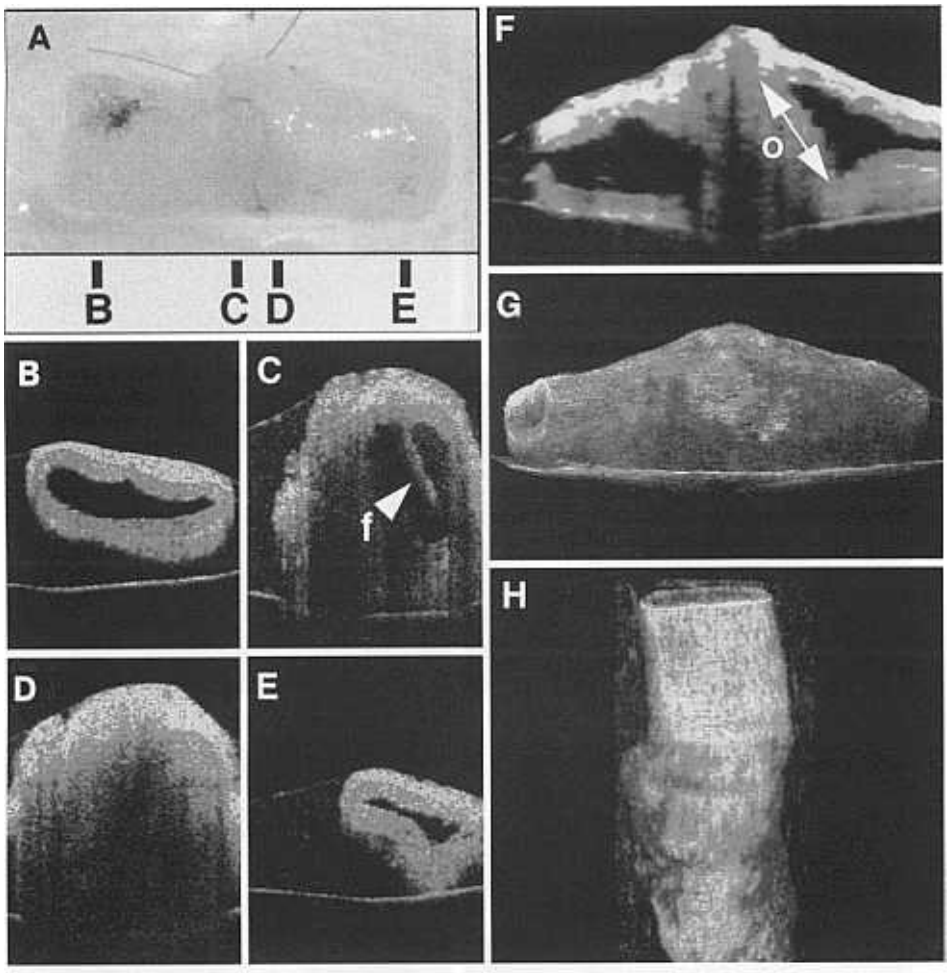

Figure 2. Three-dimensional OCT imaging of an anastomosis in a rabbit artery. *A,* Digital image obtained with a charge-coupled–device camera shows the 1-mm-diameter artery, which was anastomosed with a continuous suture. Lines labeled *B, C, D,* and *E* indicate planes from which corresponding cross-sectional OCT images were obtained. *B* and *E,* At the opposite ends of the anastomosis, the multilayered structure of the artery is visible, and the lumen is patent. *C,* Lumen is partially obstructed and a thrombogenic flap (arrowhead, *f*) is present. *D,* Fully obstructed portion of the anastomotic site is seen. Intraluminal features such as those in *C* and *D* are not observable on the en face view in *A*. *F,* Longitudinal section of the artery shows the obstruction (double-headed arrow, *o*). *G* and *H,* 3D projections can be arbitrarily constructed in any orientation, such as the horizontal (*G*) and vertical (*H*) orientations.

from animal and human tissue. Segments of inguinal-area arteries and nerves were resected from a 3.5-kg New Zealand White rabbit immediately after the rabbit was euthanized with a 5-mL injection of pentobarbital sodium (65 mg/mL). The specimens were immediately placed in 0.9% normal saline and were stored at 0°C. An artery segment was bisected cross-sectionally with a scalpel and was then reanastomosed. A 10-0 nylon suture with a 50-μm-diameter needle was used to place a continuous suture and to perform an end-to-end anastomosis.

For the precise registration of 3D images, the anastomosed segment was positioned on a micrometer-stepping, computer-controlled, motorized translational stage in the sample arm of the OCT instrument (Fig 1, *A*). The OCT imaging beam was held fixed as motorized stages translated the specimen. A series of 40 cross-sectional images were acquired perpendicular to the long axis at 100-μm intervals. Imaging was performed through the anastomotic site and several millimeters on either side of the anastomosis. After OCT imaging, the en face image of the specimen was digitally recorded with a charge-coupled–device camera. Three-dimensional imaging of the peripheral nerve was performed by using the same parameters as described for the artery. The animal used in this study was cared for and maintained under the established protocols of the Massachusetts Institute of Technology committee on animal care.

To demonstrate the ability of OCT to depict vessels and nerves embedded in highly scattering tissue in real time, a 1-cm^3 block of human tissue was removed from the left lateral ankle of an amputated foot, immediately placed in 0.9% normal saline, and stored at 0°C. The ankle had been amputated as a result of complications associated with vascular insufficiency secondary to diabetes mellitus. The block of tissue was manually manipulated under the surgical microscope (Fig 1, *B*) while OCT imaging was performed at eight frames per second in a single cross-sectional plane. Images were acquired and stored directly to S-VHS videotape while they were viewed on a monitor. The magnified imaging location was directly viewed through the surgical microscope as various locations were imaged in search of subsurface morphology. Specimens to be processed for histologic comparison were placed in 5% buffered formaldehyde immediately after imaging and were later embedded in paraffin, sectioned, and stained with hematoxylin-eosin. The protocol to use discarded tissue was approved by the committee on the use of human subjects at Massachusetts General Hospital.

Cross-sectional OCT images and 3D data-set projections were processed and displayed by using rendering software (NIH IMAGE version 1.60; National Institutes of Health, Bethesda, Md). A false-color scale was assigned to the logarithm of the data in each image in a manner analogous to that used in US. For the 40 images obtained in the peripheral nerve, a single fascicle was manually segmented and colored white on the images to en-

able tracking through the multiple sections and 3D volume. The multiple sections for each specimen were assembled into a stack and used to generate projections from the 3D data set. The projections were rotated in the x, y, and z planes to view particular features and to determine planes at which arbitrary sections could be displayed.

RESULTS

The ability to assess the internal structure and the luminal patency within an arterial anastomosis by using OCT was demonstrated by acquiring cross-sectional OCT images (2.2 × 2.2 mm, 250 × 600 pixels) and 3D projections of a 1-mm-diameter rabbit inguinal artery. A digitized image of the arterial anastomotic segment is shown in *A* in Figure 2. Cross-sectional 2D images in *B–E* in Figure 2 were acquired from the locations labeled in *A* in Figure 2. *B* and *E* in Figure 2 were acquired from each end of the anastomosis. These images clearly show the arterial morphology that corresponds to the intimal, medial, and adventitial layers of the elastic artery. The muscular media exhibits less backscatter than the adventitia, which merges with the surrounding collagenous tissue. The patent lumen is readily apparent. This is in contrast to *C* in Figure 2, where a tissue flap is seen in cross section at the site of anastomosis. *D* in Figure 2 reveals an obstruction within the arterial lumen. Note that the presence of additional tissue has attenuated the signal from the lower wall and, hence, reduces the ability to resolve individual layers.

By assembling a series of cross-sectional 2D images, a 3D data set was produced. From this data set, arbitrary planes could be selected, and corresponding sections could be displayed. For an arterial anastomosis, it is often more informative to image longitudinally along the axis of the artery and through the site of the anastomosis. *F* in Figure 2 is a longitudinal section from the 3D data set, which confirms the occlusion within the anastomotic site.

G and *H* in Figure 2 show 3D projections of the arterial anastomosis. These horizontally and vertically rotated projections comprised 80 sections at 50-μm intervals. At this high section density, the internal structure shown in *B–F* in Figure 2 is difficult to visualize. However, high section densities are necessary if the 3D data set is to be sectioned at arbitrary planes, as shown in *F* in Figure 2. In addition, micrometer-scale surface features that were not readily apparent on the 2D sections are more prominent.

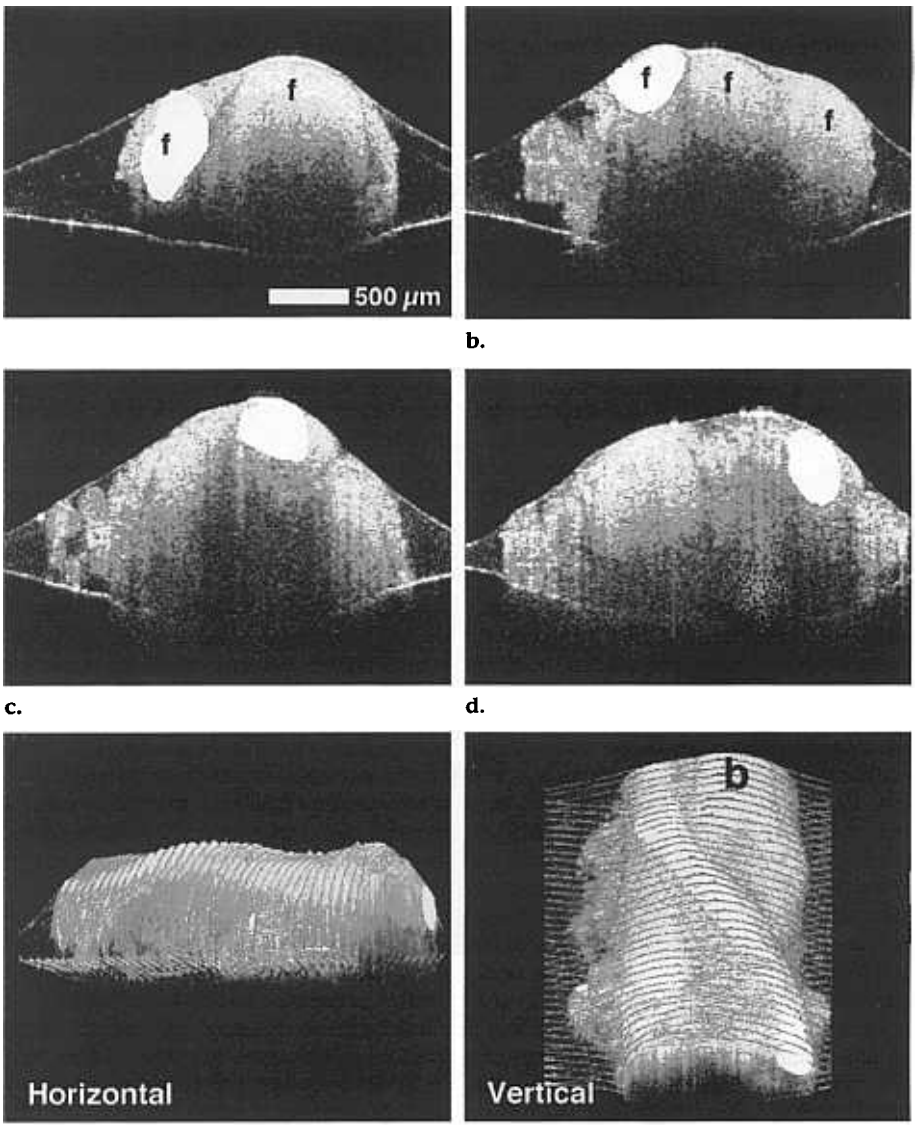

Figure 3. Three-dimensional OCT imaging of a peripheral nerve. Multiple fascicles (*f* in **a** and **b**) are evident within the peripheral nerve. **(a–d)** A single fascicle was followed longitudinally along the axis of the nerve, manually segmented, and colored white. **(e)** Horizontally and **(f)** vertically oriented 3D projections illustrate the spatial arrangement of individual fascicles and a bifurcation (*b* in **f**) not previously appreciated on 2D cross sections.

Longitudinal tracking of the spatial orientation of peripheral nerve fascicles is demonstrated in Figure 3. Representative cross-sectional images (3.0 × 2.2 mm, 300 × 600 pixels) of the peripheral nerve are shown in Figure 3a–3d. For each section, one fascicle was manually segmented, colored white, and tracked through the acquired volume of data. Forty images at 100-μm intervals were assembled for the 3D projections shown in Figure 3e and 3f. The horizontally and vertically rotated projections of the peripheral nerve dramatically reveal the twisted path of the segmented fascicle along the longitudinal axis of the nerve. In addition, a branch in another, unsegmented fascicle can be seen in Figure 3f. This feature was not recognized at the examination of the 2D images.

OCT image data was correlated with corresponding histology. Figure 4 shows cross-sectional images acquired from a rabbit arterial bifurcation and from a human retroperitoneal nerve. The arterial segment was imaged with OCT distal to the bifurcation, and two independent lumina are shown (Fig 4a). The OCT images clearly resolve individual layers within the arterial wall and demonstrate

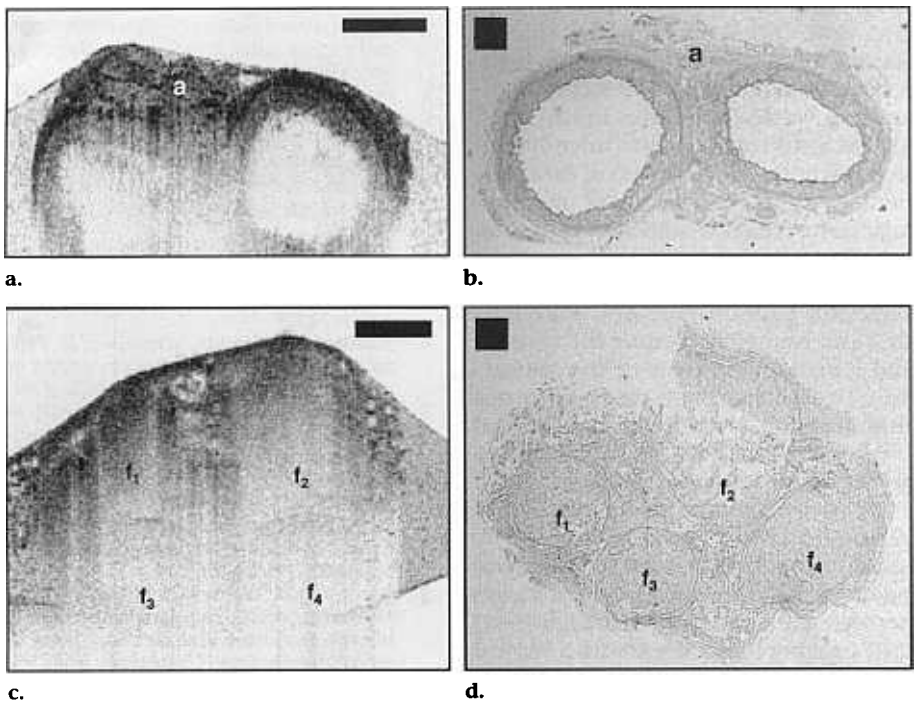

Figure 4. OCT images and corresponding histology of microsurgical specimens for correlation of image features with architectural morphology. The black bar in **a** and **c** represents 500 μm. (Disregard the black squares in **b** and **d.**) **(a)** OCT image and **(b)** photomicrograph show a bifurcation of a rabbit femoral artery, with adjacent adipose tissue (*a* in **b**). (Hematoxylin-eosin stain; original magnification, ×20.) **(c)** OCT image and **(d)** photomicrograph show multiple fascicles (f_1, f_2, f_3, f_4) in a human retroperitoneal nerve. (Hematoxylin-eosin stain; original magnification, ×20.)

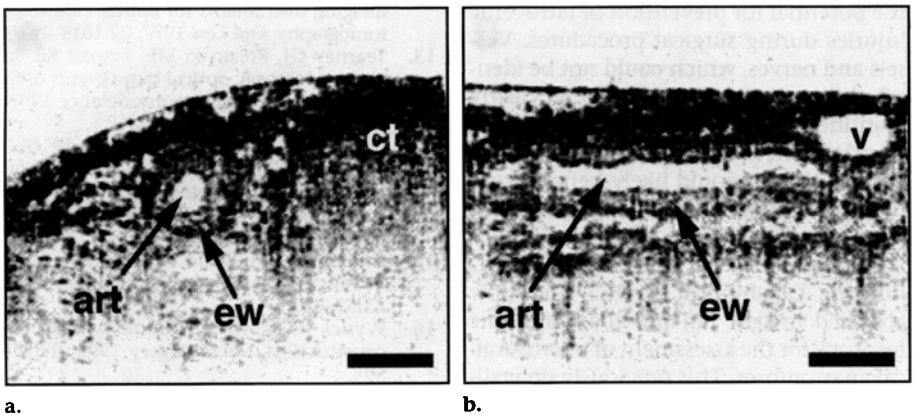

Figure 5. OCT images of a subsurface, in vitro human artery were acquired with an integrated surgical microscope at high speed (eight frames per second). The black bar in **a** and **b** represents 500 μm. **(a)** Cross-sectional image of the artery (*art*) illustrates the thick elastic wall (*ew*) and patent lumen. The artery is surrounded by adipose tissue and is adjacent to dense connective tissue (*ct*). **(b)** Longitudinal cross section of the same artery (*art*) with the thick elastic wall (*ew*) shows a thin-walled vein (*v*) in oblique cross section.

patent lumina. Above the arteries is a region of adipose tissue, which appears to have less backscatter in the OCT image, except for the nuclei and cell walls. The images of the human retroperitoneal nerve illustrate OCT imaging of individual fascicles, which correlates well with the histology (Fig 4c, 4d). Because of the larger diameter of this nerve, the OCT optical beam is attenuated, and deeper fascicles (f_3 and f_4 in Fig 4) are difficult to resolve, except for the sheath surrounding each fascicle.

The OCT instrument was integrated with a surgical microscope (Fig 1, *B*) to obtain the images shown in Figure 5. Because the OCT imaging beam and visible aiming beam were co-aligned with the optical axis of the microscope, the image location on the specimen could be directly viewed through the microscope. A block of tissue was manually manipulated under the microscope while images (3.00 × 2.75 mm, 256 × 256 pixels) were acquired at eight frames per second. Subsurface microsurgical structures were immediately identified, including numerous small arteries, veins, and nerves and even a vascular clip from previous surgical repair. All structures were embedded in adipose and connective tissues. Figure 5a illustrates a cross section of an artery located 500 μm below the surface and surrounded by adipose tissue. This artery could not be visualized with the microscope alone. The image clearly shows the characteristic thick wall and multiple layers of the artery. To the right of the artery is a portion of dense connective tissue that does not have the clear, low-backscatter regions present in adipose tissue. Figure 5b shows a longitudinal section of the same artery after the tissue block was rotated 90°. The thick arterial wall is readily identified. The right edge of Figure 5b shows an oblique cross section of a vein with its characteristic thin wall.

DISCUSSION

During microsurgical procedures, patient outcome can be substantially influenced by the ability of the surgeon to assess tissue microstructure (15). The in vitro arterial anastomosis shown in Figure 2 demonstrates the ability of OCT to help assess internal structure within an anastomotic site and evaluate patency. Precision realignment of individual nerve fascicles increases the likelihood that end-organ function will be restored after peripheral nerve reconstruction (16). With Figures 3 and 4, we showed that OCT can image peripheral nerves in cross section and that individual fascicles can be identified and segmented. The use of OCT to acquire multiple cross-sectional images and perform 3D reconstructions of the peripheral nerve offers the opportunity to determine the relative diameters of individual fascicles, as well as track their spatial orientation. The 3D projection of the segmented peripheral nerve in Figure 3f not only revealed the twisted course of one fascicle but also revealed a bifurcation of a second fascicle, a feature not previously appreciated on the 2D images.

Future work will focus on methods to increase the rate of data acquisition, to increase the resolution, and to combine structural imaging with OCT Doppler techniques. The rapid acquisition rate of eight frames per second enabled immediate feedback for repositioning of the specimen and tracking of the vessels and nerves. The current limitation to acquisition speed is the axial scanning mechanism. Use of the high-speed optical delay line has decreased image acquisition times from 30 seconds to 125 msec compared with the acquisition time achievable with a mechanical scanning galvanometer. Acquisition time can also be improved by decreasing the number of pixels in an image. We chose to acquire images with a higher resolution (256 × 256 pixels) at the expense of speed. Further improvements in axial imaging technology will enable video-rate (30 frames per second) and high-speed volume acquisition.

The image resolutions achieved in this study are as high as 10 μm and exceed the performance of clinical US, computed tomography, and magnetic resonance imaging. By using broader-bandwidth laser sources such as a titanium:sapphire Kerr-lens modelocked laser (17,18) or a Cr^{4+}: forsterite laser (14), resolutions as high as 2–5 μm may be achieved. Higher resolutions would further improve the identification of morphologic features within the anastomotic site. The maintenance of these high resolutions during performance of high-speed imaging is a current technical pursuit.

In a manner analogous to Doppler US, OCT may be configured to perform laser-Doppler velocimetry. This technique has been used for the in vivo measurement of blood flow velocities in animal models (19,20) and may be useful for the assessment of perfusion after vascular anastomosis.

Potential limitations of OCT imaging are the maximal penetration and the effect of blood on imaging. When longer wavelengths (in the near infrared range) have been used, imaging depths have increased from 1 mm up to 2–3 mm due to decreased optical absorption and scattering in tissue. These depths may appear limiting. However, the majority of microsurgical complications occur in vessels and nerves less than 2 mm in diameter and are suitable for OCT imaging. The presence of blood in the surgical field may influence the quality of OCT images. Future studies will assess the influence of blood on OCT imaging.

Practical applications: The use of a surgical microscope serves to magnify the tissue but provides only a surface, or en face, view. OCT should improve intraoperative diagnostics by providing high-resolution, subsurface, cross-sectional imaging of vessels and nerves in real time. The extension of imaging to three dimensions permits the assessment of the longitudinal spatial orientation of morphologic features such as individual peripheral nerve fascicles. Intraoperative assessment of luminal obstructions is crucial to the successful performance of a procedure. OCT can be used to identify the location and longitudinal extent of the obstruction. This would include the presence of a thrombogenic adventitial flap or intimal inversion, which predisposes the site to postoperative subacute occlusion.

We have demonstrated the capabilities of an integrated surgical microscope by acquiring in vitro images of subsurface human vessels and nerves at eight frames per second. The integration of high-speed OCT imaging components with a surgical microscope was a challenge. An aberration-free beam had to be tightly focused at a long working distance and maintained throughout the entire imaging range. Integration with the surgical microscope permitted not only en face visualization but also simultaneous cross-sectional OCT imaging. The microscope-based OCT system is a practical application of OCT technology and was used to demonstrate the potential for prevention of iatrogenic injuries during surgical procedures. Vessels and nerves, which could not be identified on en face images, were clearly identified on OCT images. Performance of many fine surgical procedures in vulnerable tissues would likely benefit from high-resolution subsurface imaging findings.

In this article, we have shown the 3D imaging capabilities of OCT and how acquired images can provide diagnostic feedback for the assessment of microsurgical anastomoses. This previously unavailable diagnostic ability offers the potential to directly affect and improve patient outcome by incorporating high-speed, high-resolution, intraoperative imaging of microsurgical procedures.

Acknowledgments: The authors thank Eric A. Swanson, MS, of Massachusetts Institute of Technology Lincoln Laboratories for helpful technical discussions and contributions and Cindy Kopf of the Massachusetts Institute of Technology for helping to assemble this manuscript.

References

1. Zhong-wei C, Dong-yue Y, Di-Sheng C, eds. Microsurgery. New York, NY: Springer-Verlag, 1982; 68–92.
2. Rooks MD, Slappey J, Zusmanis K. Precision of suture placement with microscope and loupe assisted anastomoses. Microsurgery 1993; 14:547–550.
3. Huang D, Swanson EA, Lin CP, et al. Optical coherence tomography. Science 1991; 254:1178–1181.
4. Hee MR, Izatt JA, Swanson EA, et al. Optical coherence tomography of the human retina. Arch Ophthalmol 1995; 113: 326–332.
5. Puliafito CA, Hee MR, Lin CP, et al. Imaging of macular diseases with optical coherence tomography. Ophthalmology 1995; 120:217–229.
6. Puliatifo CA, Hee MR, Schumann JS, Fujimoto JG. Optical coherence tomography of ocular diseases. Thorofare, NJ: SLACK, 1995.
7. Fujimoto JG, Brezinski ME, Tearney GJ, et al. Optical biopsy and imaging using optical coherence tomography. Nat Med 1995; 1:970–972.
8. Schmitt JM, Yadlowsky M, Bonner RF. Subsurface imaging of living skin with optical coherence microscopy. Dermatology 1995; 191:93–98.
9. Brezinski ME, Tearney GJ, Bouma BE, et al. Optical coherence tomography for optical biopsy: properties and demonstration of vascular pathology. Circulation 1996; 93: 1206–1213.
10. Brezinski ME, Tearney GJ, Boppart SA, Swanson EA, Southern JF, Fujimoto JG. Optical biopsy with optical coherence tomography: feasibility for surgical diagnostics. J Surg Res 1997; 71:32–40.
11. Tearney GJ, Boppart SA, Bouma BE, et al. Scanning single-mode fiber optic catheter-endoscope for optical coherence tomography. Opt Lett 1996; 21:543–545.
12. Boppart SA, Bouma BE, Pitris C, Tearney GJ, Fujimoto JG, Brezinski ME. Forward-imaging instruments for optical coherence tomography. Opt Lett 1997; 22:1618–1620.
13. Tearney GJ, Brezinski ME, Bouma BE. In vivo endoscopic optical biopsy with optical coherence tomography. Science 1997; 276:2037–2039.
14. Bouma BE, Tearney GJ, Bilinsky IP, Golubovic B, Fujimoto JG. Self-phase modulated Kerr-lens modelocked Cr^{4+}: forsterite laser source for optical coherence tomography. Opt Lett 1996; 21:1839–1841.
15. Culbertson JH, Rand RP, Jurkiewicz MJ. Advances in microsurgery. Adv Surg 1990; 23:57–88.
16. Wyrick JD, Stern PJ. Secondary nerve reconstruction. Microsurgery 1992; 8:587–598.
17. Bouma BE, Tearney GJ, Boppart SA, Hee MR, Brezinski ME, Fujimoto JG. High resolution optical coherence tomographic imaging using a modelocked Ti:Al_2O_3 laser source. Opt Lett 1995; 20:1486–1488.
18. Clivaz X, Marquis-Weible F, Salathe RP. Optical low coherence reflectometry with 1.9 μm spatial resolution. Electronics Lett 1992; 28:1553–1555.
19. Chen Z, Milner TE, Srinivas S, Wang X. Noninvasive imaging of in vivo blood flow velocity using optical Doppler tomography. Opt Lett 1997; 22:1119–1121.
20. Izatt JA, Kulkami MD, Yazdanfar S, Barton JK, Welch AJ. In vivo bidirectional color Doppler flow imaging of picoliter blood volumes using optical coherence tomography. Opt Lett 1997; 22:1439–1441.